

Focus FMCW SAR Data Using the Wavenumber Domain Algorithm

Robert Wang, *Member, IEEE*, Otmar Loffeld, *Senior Member, IEEE*, Holger Nies, Stefan Knedlik, *Member, IEEE*, Manfred Hägelen, and Helmut Essen

Abstract—The combination of frequency-modulation continuous-wave (FMCW) technology and synthetic aperture radar (SAR) promises a lightweight, cost-effective, and high-quality imaging sensor for remote sensing. However, the long signal duration time leads to the failure of the conventional start/stop approximation of the pulsed SAR. In this paper, a signal model is proposed to address the effects of the continuous motion during the transmit time on the echoed signal. Based on the model, an analytical point target reference spectrum is derived. From the spectrum, it will be seen that the continuous motion introduces an additional range–azimuth coupling term and a range walk term compared with the conventional pulsed SAR. The range walk term is well known, whereas the foregoing range–azimuth coupling term is formulated for the first time in the FMCW SAR community. For the squint and spotlight modes, these range walk and range–azimuth coupling terms might significantly degrade the image quality. In this paper, based on the proposed analytical signal model, we further discuss the application of the wavenumber domain algorithm for the FMCW SAR data. In addition, different approximations of the Stolt mapping are made to highlight the effect of the range-dependent higher-order range–azimuth coupling terms on the 2-D impulse responses. Finally, X-band simulated experiments and Ka-band real FMCW SAR data are used to validate the signal model and the processing method.

Index Terms—Frequency-modulation continuous wave (FMCW), point target reference spectrum (PTRS), range cell migration correction (RCMC), wavenumber domain algorithm (WDA).

I. INTRODUCTION

CONVENTIONAL synthetic aperture radar (SAR) works in pulsed mode [1]. Continuous-wave technology, however, requires less peak transmit power [2], [3]. Hence, frequency-modulation continuous-wave (FMCW) SAR offers the benefits of compact size and low cost. However, it is currently applied only in the short-range case.

For FMCW SAR, the variation of the instantaneous slant range introduced by the continuous motion during the pulse time is no longer negligible since the conventional start/stop approximation does not hold. Conceptually, this start/stop ap-

proximation assumes that any transmitted pulse experiences a delay time, which is constant during the pulse duration and only varies from pulse to pulse (known as range migration), whereas in principle, leading edge and trailing edge of any transmitted pulse experience different delay times introduced by the time-varying slant range. Therefore, processing of FMCW SAR differs from the conventional pulsed SAR due to the fact that the range walk term and an additional range–azimuth coupling are introduced by the continuous motion of the antenna while transmitting and receiving the signal. The range walk term is discussed in detail in [3], whereas the additional range–azimuth coupling term is not mentioned. Therefore, conventional SAR algorithms cannot directly be applied. Recently, several conventional algorithms have been modified to focus FMCW SAR data [3]–[7]. The range-Doppler algorithm has been modified to focus FMCW SAR data in [4]. In [4], the continuous motion within the sweep is discussed and compensated by modifying the range migration compensation. Meta *et al.* [5] present a nonlinear frequency-scaling algorithm, which simultaneously performs the nonlinear correction, Doppler-shift correction, and range cell migration correction (RCMC) in the wavenumber domain. It can be considered as an extension of the result proposed in [6]. In addition, a chirp transformation algorithm is also used to process FMCW SAR data [7]. The aforementioned three methods neglect the range-dependent second- and higher-order range–azimuth coupling terms that play a key role in the squint or spotlight modes.

In this paper, we begin with a signal model, which accurately represents the effect of the variation of the instantaneous slant range during the pulse time on the transmitted and echoed signal. This variation during the transmitting time introduces a range-invariant range walk and a range–azimuth coupling. The range walk is corrected by a phase multiplication, which can be incorporated into the reference function multiplication (RFM) [9]. RFM is applied in the 2-D frequency domain. It works as a bulk compressor [9] and is responsible for the range-independent range walk, high-order range frequency terms, and azimuth compression. After RFM, we perform the Stolt interpolation in the wavenumber domain [8], [9]. The Stolt interpolation can correct the range-dependent RCM and cancel the range-dependent higher-order range–azimuth coupling terms and azimuth modulation. Therefore, it is suitable to process the FMCW SAR in the spotlight and high-squint modes. To demonstrate the performance of the wavenumber domain algorithm (WDA), the different approximations of the Stolt mapping are used to highlight the effect of the range-dependent higher-order range–azimuth coupling components on 2-D focusing. In this paper, our processing procedure proceeds with the removal of

Manuscript received May 12, 2009; revised July 5, 2009 and July 27, 2009.

R. Wang, O. Loffeld, H. Nies, and S. Knedlik are with the Center for Sensorsystems (ZESS), University of Siegen, 57076 Siegen, Germany (e-mail: wang@zess.uni-siegen.de; loffeld@zess.uni-siegen.de; nies@zess.uni-siegen.de; knedlik@zess.uni-siegen.de).

M. Hägelen and H. Essen are with the Fraunhofer Institute for High Frequency Physics and Radar Techniques (FHR), 53343 Wachtberg, Germany (e-mail: m.haegelen@fgan.de; essen@fgan.de).

Color versions of one or more figures in this paper are available online at <http://ieeexplore.ieee.org>.

Digital Object Identifier 10.1109/TGRS.2009.2034368

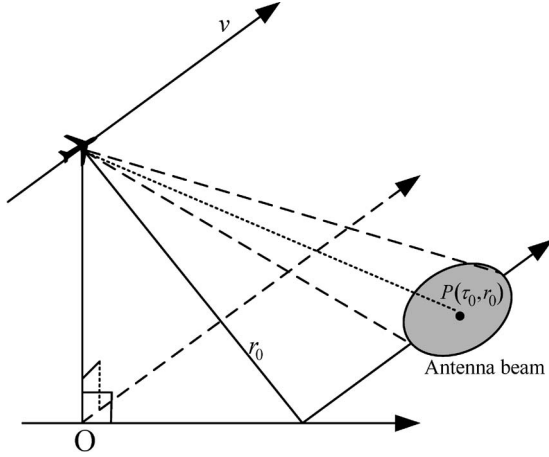


Fig. 1. Geometry of the SAR system.

the residual video phase (RVP), which is introduced by the applied dechirp-on-receive operation. The compensation of the RVP has been discussed in detail in [10] and [11].

This paper is organized as follows. In Section II, the signal model and the point target reference spectrum (PTRS) are derived. Section III begins with the spectrum and uses the WDA for processing FMCW SAR data. Hereafter, we show the processing results of simulated raw data in Section IV and of real FMCW SAR data in Section V. Finally, conclusions are reported in Section VI.

II. SIGNAL MODEL AND PTRS

In this paper, we consider the general SAR geometry, as shown in Fig. 1.

The mathematical symbols and their definitions used in this paper are given as follows.

| | |
|-----------------------|---|
| τ, t | Azimuth and range time variables. |
| r_0 | Closest ranges from the antenna to the target $P(\tau_0, r_0)$. |
| r_c | Reference slant range for the dechirp-on-receive approach. |
| τ_0 | Zero-Doppler time of the target $P(\tau_0, r_0)$. |
| $\sigma(\tau_0, r_0)$ | Backscattering coefficient of the point target $P(\tau_0, r_0)$. |
| r_m | Closest range from the scene center to the flight trajectory. |
| λ, f_0 | Carrier wavelength and carrier frequency of the transmitted signal. |
| c | Speed of light. |
| f, f_τ | Range and azimuth frequency variables. |
| K_r | Chirp rate of the transmitted signal. |
| T_p | Pulse repetition period. |

In the pulsed SAR, the start/stop approximation is commonly used, where the instantaneous slant range from the antenna to the target is assumed to remain constant during the pulse time. In the case of the continuous-wave (CW) SAR, however, the instantaneous slant range can no longer be assumed constant due to the long signal duration. To develop the signal model for the CW SAR system, we first perform an analysis of the round-trip delay time. Let the time τ_d be the round-trip delay time for

the wave propagation. The signal is transmitted at an arbitrary time τ at an instantaneous slant range $R(\tau)$ and arrives back at the receiver at time $\tau + \tau_d$, having traveled along the slant range from the target to the receiver $R(\tau + \tau_d)$. Thus, we can express the round-way delay time as

$$\frac{R(\tau + \tau_d) + R(\tau)}{c} = \tau_d \quad (1)$$

where

$$R(\tau) = \sqrt{r_0^2 + v^2(\tau - \tau_0)^2} \quad (2)$$

$$R(\tau + \tau_d) = \sqrt{r_0^2 + v^2(\tau + \tau_d - \tau_0)^2}. \quad (3)$$

Shifting $R(\tau)/c$ to the right-hand side and squaring both sides, we can obtain a quadratic equation in terms of τ_d . By solving the quadratic equation for τ_d , we obtain

$$\tau_d = 2\alpha \left[\frac{R(\tau)}{c} + \frac{v^2}{c^2}(\tau - \tau_0) \right] \quad (4)$$

where the “Doppler factor” α is defined as

$$\alpha = \frac{1}{1 - \frac{v^2}{c^2}}. \quad (5)$$

By using (4), and neglecting the timescaling influences on the pulse envelope, the echoed signal can be expressed as

$$g_r(\tau, t, r_0, s_0) = \sigma(\tau_0, r_0) s_l(t - \tau_d) \exp[j2\pi f_0(t - \tau_d)] \quad (6)$$

where $s_l(t)$ represents the transmitted FM signal, which is defined as $s_l(t) = \exp(j\pi K_r t^2)$. Since the SAR is time coherent, the transmitted signal is synchronized by the repetition period, i.e., $t = \tau - nT_p$. The signal is transmitted at the time $\tau_n = nT_p$, where n denotes the period number.

In the pulsed mode, the pulse duration is short on the order of a few microseconds; however, for the FMCW mode, the pulse duration is on the order of milliseconds, corresponding to the pulse repetition interval. The dechirp-on-receive technology is generally used in the FMCW SAR system to reduce the sampling requirements and data rate [3], [10]. The reference signal for dechirp processing is defined as

$$g_{\text{ref}}(\tau, t, t_c) = s_l^*(t - \tau_c) \exp[-j2\pi f_0(t - \tau_c)] \quad (7)$$

where $s_l^*(t)$ denotes the conjugate of the transmitted signal $s_l(t)$, and τ_c is the time delay of the reference signal. For notational convenience, τ_c is defined as $\tau_c = 2\alpha r_c/c$. The dechirped signal can be expressed as

$$\begin{aligned} g_{\text{IF}}(\tau, t, r_0, \tau_0) &= g(\tau, t, r_0, \tau_0) \times g_{\text{ref}}(\tau, t, t_c) \\ &= \sigma(\tau_0, r_0) \exp[-j2\pi f_0(\tau_d - \tau_c)] \\ &\quad \times \exp[-j2\pi K_r(\tau_d - \tau_c)(t - \tau_c)] \\ &\quad \times \exp[-j2\pi K_r(\tau_d - \tau_c)^2]. \end{aligned} \quad (8)$$

The last exponential term of (8) is well known as an RVP [10]. Removing the RVP needs Fourier transformation (FT), phase multiplication, and inverse FT (IFT) [10], [11]. The

following derivation assumes that the RVP has been removed, i.e.,

$$g_{IF}(\tau, t, r_0, \tau_0) = \sigma(\tau_0, r_0) \exp[-j2\pi f_0(\tau_d - \tau_c)] \times \exp[-j2\pi K_r(\tau_d - \tau_c)(t - \tau_c)]. \quad (9)$$

Performing the time–frequency substitution of $K_r(t - \tau_c) \rightarrow f$ yields

$$g_{IF}(\tau, f, r_0, \tau_0) = \sigma(\tau_0, r_0) \times \exp[-j2\pi(f_0 + f)(\tau_d - \tau_c)]. \quad (10)$$

To segment the received signal into the 2-D discrete domain, we substitute $\tau = \tau_n + t$ into (10). Equation (10) can then be reformulated as

$$\begin{aligned} g_{IF}(\tau_n, t, f, r_0, \tau_0) &= \sigma(\tau_0, r_0) \\ &\times \exp \left\{ -j4\pi\alpha(f_0 + f) \right. \\ &\times \left[\frac{R(\tau_n + t)}{c} + \frac{v^2}{c^2}(\tau_n + t - \tau_0) - \frac{r_c}{c} \right] \left. \right\}. \quad (11) \end{aligned}$$

To obtain the PTRS, we apply the FT to (11) with respect to the discrete-time variable τ_n , i.e.,

$$\begin{aligned} G_{IF}(f_\tau, t, f, r_0, \tau_0) &= \int g_{IF}(\tau_n, t, f, r_0, \tau_0) \\ &\times \exp[-j2\pi f_\tau \tau_n] d\tau_n = \sigma(\tau_0, r_0) \int \exp[-j\Phi(f_\tau, f, \tau_n)] d\tau_n \end{aligned} \quad (12)$$

where $\Phi(f_\tau, f, \tau_n)$ is defined as

$$\begin{aligned} \Phi(f_\tau, t, f, \tau_n) &= 4\pi\alpha(f_0 + f) \\ &\times \left[\frac{R(\tau_n + t)}{c} + \frac{v^2}{c^2}(\tau_n + t - \tau_0) - \frac{r_c}{c} \right] + 2\pi f_\tau \tau_n. \quad (13) \end{aligned}$$

Consequently, the principle of stationary phase can readily be applied to obtain the solution of the integral to derive the desired PTRS. At the point of stationary phase, the first derivative of the phase $\Phi(f_\tau, f, \tau_n)$ is zero, i.e.,

$$\left. \frac{d\Phi(f_\tau, t, f, \tau_n)}{d\tau_n} \right|_{\tau_n=\tau_p} = 0. \quad (14)$$

Solving (14) for τ_p yields

$$\tau_p = \tau_0 - \frac{\frac{r_0}{v} \left[\frac{v}{c} + \frac{cf_\tau}{2\alpha v(f_0 + f)} \right]}{\sqrt{1 - \left[\frac{v}{c} + \frac{cf_\tau}{2\alpha v(f_0 + f)} \right]^2}} - t. \quad (15)$$

Substituting τ_p on the right-hand side of (12) for τ_n gives the desired PTRS (The nonessential amplitude and phase terms are disregarded.). Thus

$$G_{IF}(f_\tau, f, r_0, s_0) = \sigma(\tau_0, r_0) \exp[-j\Phi(f_\tau, f, r_0)] \quad (16)$$

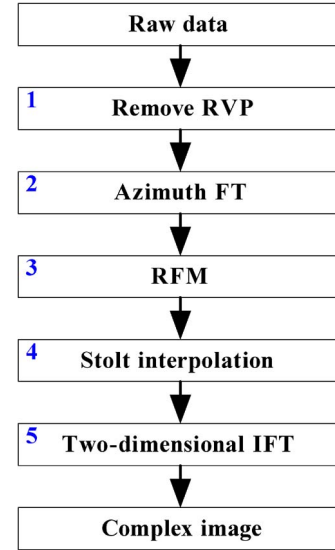


Fig. 2. Block diagram of the focusing algorithm.

where the phase term in the 2-D frequency domain can be expressed as (note that the substitution $K_r(t - \tau_c) \rightarrow f$ is further introduced)

$$\begin{aligned} \Phi(f_\tau, f, r_0) &= \frac{4\pi\alpha r_0}{c} \sqrt{(f_0 + f)^2 - \left[\frac{v}{c}(f_0 + f) + \frac{cf_\tau}{2\alpha v} \right]^2} \\ &- 2\pi f_\tau \frac{f}{K_r} + 2\pi f_\tau \tau_0 - 4\pi\alpha(f_0 + f) \frac{r_c}{c} - 4\alpha\pi \frac{r_c}{c} f_\tau. \quad (17) \end{aligned}$$

Some short remarks concerning (17) will be helpful to understand the characteristics of this FMCW SAR.

- 1) The square root contains the additional term $(v/c)(f_0 + f)$, which is not presented in the pulsed SAR PTRS [9]. It adds a range–azimuth coupling in the 2-D frequency domain, which results in the skewness of the 2-D spectrum along the range frequency direction [9]. It is introduced by the variation of the slant range during the long pulse duration. This coupling term is the basic difference between this proposed spectrum and the one presented in [3], where it is neglected.
- 2) The second term in (17) (i.e., $-2\pi(f_\tau/K_r)f$) is a range-invariant range walk term, which is also caused by the variation of the slant range during the pulse duration.
- 3) $2\pi f_\tau \tau_0$ is linearly dependent on the zero-Doppler time of the target and thus determines the azimuth registration position of the target after azimuth compression.

The last two terms, i.e., $4\pi\alpha(f_0 + f)(r_c/c)$ and $2\pi f_\tau(2r_c/c)$, refer to the constant range and azimuth shifts, respectively, and are introduced by the dechirp-on-receive approach. They can be removed by using RFM.

III. PROCESSING PROCEDURE

This section provides the processing steps of the proposed algorithm shown in Fig. 2 and illustrates its basic operation.

The basic steps are outlined in the list that follows.

- 1) Remove RVP. This operation requires the range FT, chirp phase multiplication, and range IFT. It is described in detail in [10] and [11].
- 2) Perform the FT in the azimuth to transform the raw data into the 2-D frequency domain.
- 3) RFM. It is carried out to remove the range-invariant phase (i.e., bulk range walk, constant azimuth shift, azimuth modulation, bulk RCM, and bulk secondary range compression (SRC) [9]). Thus, the RFM filter can be expressed as

$$H_{\text{RFM}}(f_\tau, f, r_{\text{ref}}) = \exp[j\Phi_R(f_\tau, f, r_{\text{ref}})] \quad (18)$$

where $\Phi_R(f_\tau, f, r_{\text{ref}})$ is defined as

$$\Phi_R(f_\tau, f, r_{\text{ref}}) = \frac{4\pi\alpha r_{\text{ref}}}{c} \sqrt{(f_0 + f)^2 - \left[\frac{v}{c}(f_0 + f) + \frac{cf_\tau}{2\alpha v} \right]^2} - 2\pi f_\tau \frac{f}{K_r} - 4\pi\alpha(f_0 + f) \frac{r_c}{c} - 4\pi\alpha \frac{r_c}{c} f_\tau \quad (19)$$

where r_{ref} denotes the reference range for focus processing, which is generally defined as the closest slant range from the scene center to the receiver. Via RFM filtering, the targets at the reference range are correctly focused, but the targets away from the range are only partially focused [9]. After RFM filtering, the remaining signal becomes

$$G_1(f_\tau, f, r_0, \tau_0) = G_{\text{IF}}(f_\tau, f, r_0, \tau_0) \times H_{\text{RFM}}(f_\tau, f, r_{\text{ref}}) = \sigma(\tau_0, r_0) \exp[-j\Phi_{\text{RFM}}(f_\tau, f, r_0)] \quad (20)$$

where $\Phi_{\text{RFM}}(f_\tau, f, r_0)$ is formulated as

$$\Phi_{\text{RFM}}(f_\tau, f, r_0) = \frac{4\pi\alpha(r_0 - r_{\text{ref}})}{c} \times \sqrt{(f_0 + f)^2 - \left[\frac{v}{c}(f_0 + f) + \frac{cf_\tau}{2\alpha v} \right]^2} - 2\pi f_\tau \tau_0. \quad (21)$$

From (21), it can be seen that the range walk caused by the continuous motion is removed by RFM.

- 4) Perform the Stolt interpolation. After removing the range walk, the conventional WDA can directly be applied to focus FMCW SAR data. For the WDA, the Stolt interpolation needs to be performed to remap the range frequency variable and is formulated as

$$\sqrt{(f_0 + f)^2 - \left[\frac{v}{c}(f_0 + f) + \frac{cf_\tau}{2\alpha v} \right]^2} \rightarrow f_0 + f_1. \quad (22)$$

For the traditional pulsed SAR processing, the Stolt interpolation is defined as [9]

$$\sqrt{(f_0 + f)^2 - \left(\frac{cf_\tau}{2v} \right)^2} \rightarrow f_0 + f_1. \quad (23)$$

Therefore, the additional range–azimuth coupling term in the Stolt variable is the essential difference between

the traditional pulsed SAR and the FMCW SAR. In [12], another Stolt interpolation is presented, which is given as

$$\sqrt{\alpha(f + f_0)^2 - \frac{1}{\alpha} \left[\frac{v}{c}(f + f_0) - \frac{cf_\tau}{2\alpha v} \right]^2} \rightarrow f_0 + f_1. \quad (24)$$

The Stolt variable involved in (24) is derived based on the assumption that the time from the transmitter to the target is equal to half of the round-trip delay. In fact, as stated in the footnote of [12], it is an approximation, whereas (22) is obtained based on the analytical derivations shown in (1)–(4). After the remapping transformation, the resulting phase is now linearly dependent on the new range frequency variable f_1 , i.e.,

$$\Phi_{\text{Stolt}}(f_\tau, f, r_0) = -\frac{4\pi\alpha(r_0 - r_{\text{ref}})}{c} (f_0 + f_1) - 2\pi f_\tau \tau_0. \quad (25)$$

From (25), we can find that the Stolt interpolation completely removes the range–azimuth coupling and azimuth modulation.

- 5) Transform the signal into the complex image domain by performing the 2-D IFT. We obtain

$$g_1(\tau, t, \tau_0, r_0) = p_r \left(t - \frac{2\alpha(r_0 - r_{\text{ref}})}{c} \right) p_a(\tau - \tau_0) \quad (26)$$

where $p_r(t)$ and $p_a(\tau)$ are the compressed pulse envelope in the range and the azimuth, respectively.

From (22), it can be seen that no approximations have been performed for the RCMC and SRC. Hence, it has an advantage of precisely correcting the range-dependent second- and higher-order range–azimuth coupling terms, regardless of the squint or the aperture width.

The range-dependent second- and higher-order range–azimuth coupling terms not only result in the range focusing degradation but also defocus the azimuth impulse response since they also contain azimuth modulation components. The involved azimuth modulation components can be understood by expanding (21) using a Taylor series, i.e.,

$$\begin{aligned} \Phi_{\text{RFM}}(f_\tau, f, r_0) &\approx \frac{4\pi\alpha(r_0 - r_{\text{ref}})}{c} \\ &\times \left[Df_0 + \frac{(1 - \mu_1\mu_2)}{D} f - \frac{(\mu_1 - \mu_2)^2}{2f_0 D^3} f^2 \right. \\ &\quad \left. + \frac{(\mu_1 - \mu_2)^2(1 - \mu_1\mu_2)}{2f_0^2 D^5} f^3 + \dots \right] - 2\pi f_\tau \tau_0 \quad (27) \end{aligned}$$

where D denotes the cosine of the instantaneous squint angle in the Doppler domain and is defined as

$$D = \sqrt{1 - \mu_1^2}. \quad (28)$$

The parameters μ_1 and μ_2 are formulated as

$$\mu_1 = \frac{v}{c} + \frac{cf_\tau}{2\alpha v} \quad \mu_2 = \frac{v}{c}. \quad (29)$$

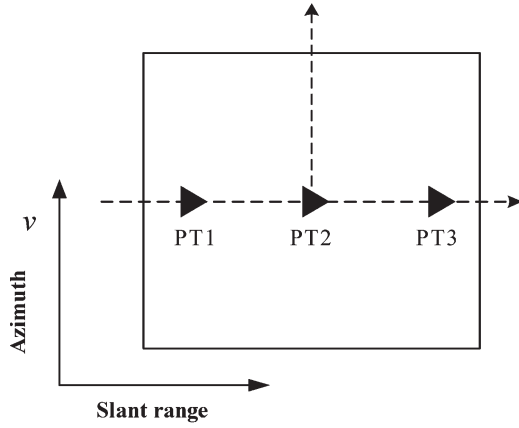


Fig. 3. Scene geometry with three point targets. Target PT2 is located in the scene center. PT1 and PT3 have the relative slant ranges: -150 and 150 m, respectively, with respect to PT2.

TABLE I
SYSTEM PARAMETERS

| | |
|-----------------------|--------------|
| Carrier frequency | 10.0 GHz |
| Range bandwidth | 500 MHz |
| PRF | 700 Hz |
| Velocity | 45 m/s |
| Azimuth beamwidth | 2.5° |
| Squint angle | $0/40^\circ$ |
| Mid-swath slant range | 800 m |
| Swath width | 400 m |
| Sampling frequency | 1.2 MHz |

For the methods in [4], [5], and [7], the effect of the second- and higher-order terms are neglected. It means that (27) is terminated after the first-order term and is given as

$$\Phi_{\text{RFM}}(f_\tau, f, r_0) \approx \frac{4\pi\alpha(r_0 - r_{\text{ref}})}{c} \times \left[Df_0 + \frac{(1 - \mu_1\mu_2)}{D}f \right] - 2\pi f_\tau \tau_0. \quad (30)$$

The approximation involved in (30) can be considered as their limitation. In the following section, we will highlight the limitation using a simulation experiment.

IV. SIMULATION EXPERIMENT

In this section, an airborne simulation is carried out to validate the performance of the present methods and analyze the effect of the higher-order range–azimuth coupling terms. To highlight the range dependence of the PTRS and the focusing capacity of the WDA, the designed scene consists of three point targets orthogonal to the flight direction, as shown in Fig. 3. The system parameters are listed in Table I.

In this experiment, different broadside and squint configurations are simulated to highlight the role of the higher-order range–azimuth coupling terms. To quantify the precision of processing, the impulse response width (IRW), peak sidelobe ratio (PSLR), and integrated sidelobe ratio (ISLR) are used as criteria. For the ongoing simulation, we assume the window function of rectangular shape in both directions.

A. Broadside Configuration

In the broadside configuration, the ideal IRW is 0.3 m in range and 0.343 m in azimuth. In the following, we perform the two kinds of Stolt interpolation transformation.

- 1) Case 1: an approximated interpolation neglecting the second- and higher-order coupling terms, i.e.,

$$\left[Df_0 + \frac{(1 - \mu_1\mu_2)}{D}f \right] \rightarrow f_0 + f_1. \quad (31)$$

- 2) Case 2: the Stolt interpolation described by (22).

1) *Case 1*: The first interpolation transformation is based on the approximation of (30), which neglects the second- and higher-order coupling terms. The resulting phase error can be expressed as

$$\Phi_E(f_\tau, f, r_0) \approx \frac{4\pi\alpha(r_0 - r_{\text{ref}})}{c} \times \left[\sqrt{(f_0 + f)^2 - \left[\frac{v}{c}(f_0 + f) + \frac{cf_\tau}{2\alpha v} \right]^2} - Df_0 - \frac{(1 - \mu_1\mu_2)}{D}f \right]. \quad (32)$$

The focused result using the transformation of (31) is shown in Fig. 4(a).

To examine the focusing performance in more detail, the point target PT3 is highlighted, and the contour of the target energy is shown in Fig. 4(b). From Fig. 4(b), it can be seen that the 2-D measured parameters agree well with the theoretical values, which means that the ignored second- and higher-order phase-coupling terms do not seriously degrade the focusing performance. This phenomenon can be explained using the approximation phase error term (32), which is shown in Fig. 4(c).

From Fig. 4(c), we can find that the maximum of the phase error is less than 0.1π , i.e., $|\Phi_E| < 0.1\pi$, which satisfies an acceptable level of $\pi/4$ [9]. Therefore, in this case, it is reasonable to neglect the second- and higher-order terms in (31). This is also the right reason that the preceding three methods (i.e., [4], [5], and [7]) achieve satisfactory focusing results.

2) *Case 2*: This interpolation transformation is the original Stolt interpolation [8], [9]. The resulting focusing result is shown in Fig. 4(d). To observe more clearly, the 2-D impulse response of PT3 is shown in Fig. 4(e).

From Fig. 4(e), it can be seen that the WDA also focuses the simulated scene well in the broadside case. Comparing Fig. 4(b) and (e), we may note that the second- and high-order range–azimuth coupling components almost have no effect on the 2-D impulse response in the broadside case.

B. High-Squint Configuration

In the squint configuration of 40° , the ideal IRW is 0.3 m in range and 0.4485 m in azimuth. We use three interpolation transformations to demonstrate the performance of the WDA and highlight the role of the second- and higher-order range–azimuth coupling terms.

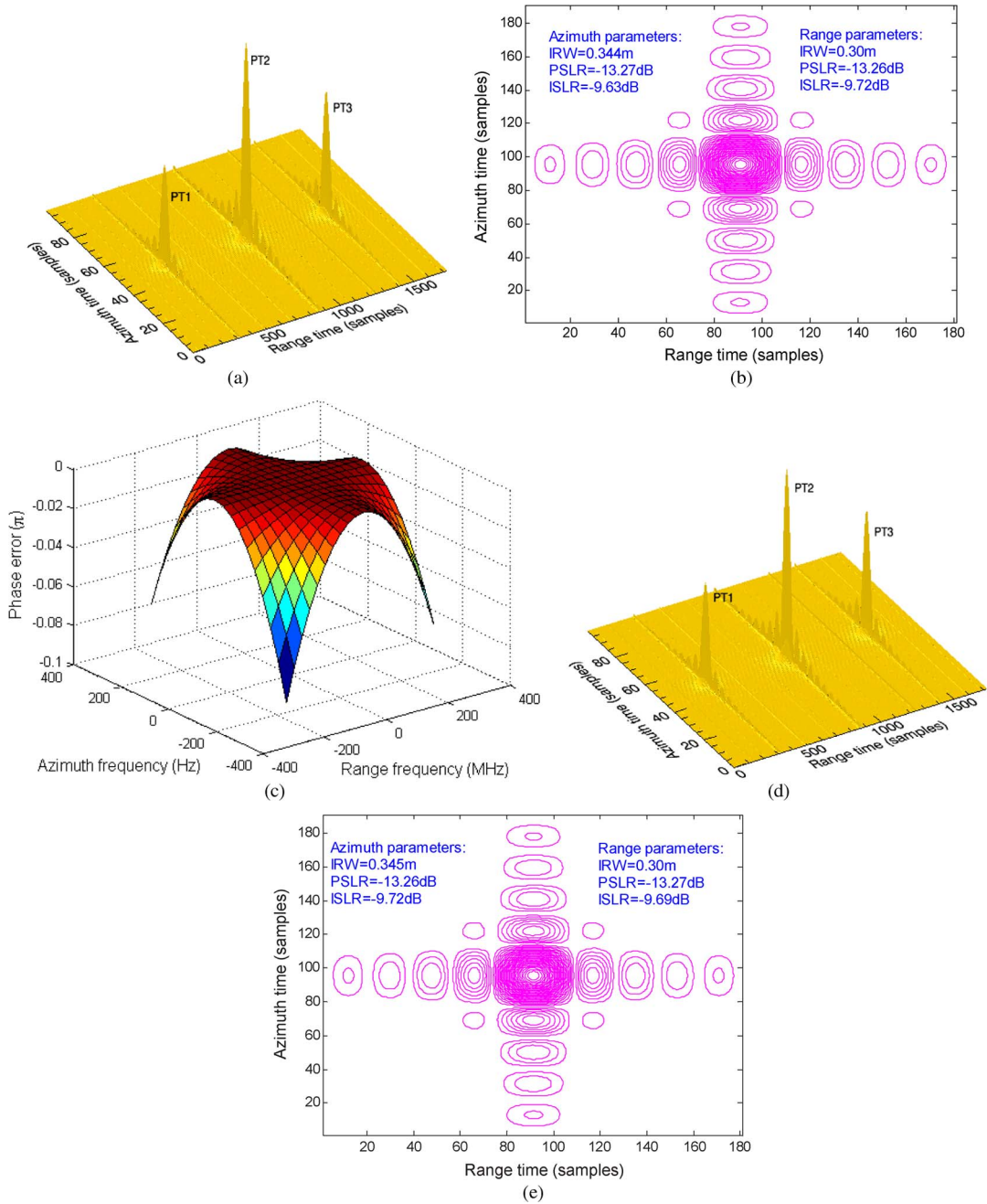


Fig. 4. (a) Focused scene processed using the interpolation transformation of (18) in the broadside configuration. (b) Impulse responses of target PT3. (c) Approximation phase error of PT3 in the broadside configuration. (d) Focused scene processed using the interpolation transformation of (18) in the broadside configuration. (e) Impulse responses of target PT3.

- 1) Case 1: the first-order polynomial interpolation transformation, i.e., (31).
- 2) Case 2: the Stolt interpolation, i.e., (22).
- 3) Case 3: the third-order polynomial interpolation transformation, i.e.,

$$\left[Df_0 + \frac{(1 - \mu_1\mu_2)}{D}f - \frac{(\mu_1 - \mu_2)^2}{2f_0D^3}f^2 + \frac{(\mu_1 - \mu_2)^2(1 - \mu_1\mu_2)}{2f_0^2D^5}f^3 \right] \rightarrow f_0 + f_1. \quad (33)$$

1) *Case 1:* First, we show the focusing result by using (31) in Fig. 5(a).

From Fig. 5(a), it can be seen that the targets away from the swath center considerably degrade in both directions. The degradations imply that the neglected range–azimuth coupling components have a significant effect on the 2-D impulse responses. To clearly identify the effect of the phase error, we show the approximation phase error of PT3 in Fig. 5(b).

Fig. 5(b) shows that the maximum of the approximation phase error $|\Phi_E|$ is greater than 10π , which is much more than the acceptable level of $\pi/4$ [9]. It is caused by the neglected higher-order range–azimuth coupling components.

The methods proposed in [4], [5], and [7] are originally designed for swath SAR zero-Doppler processing and thus neglect higher-order range–azimuth coupling components. Apparently,

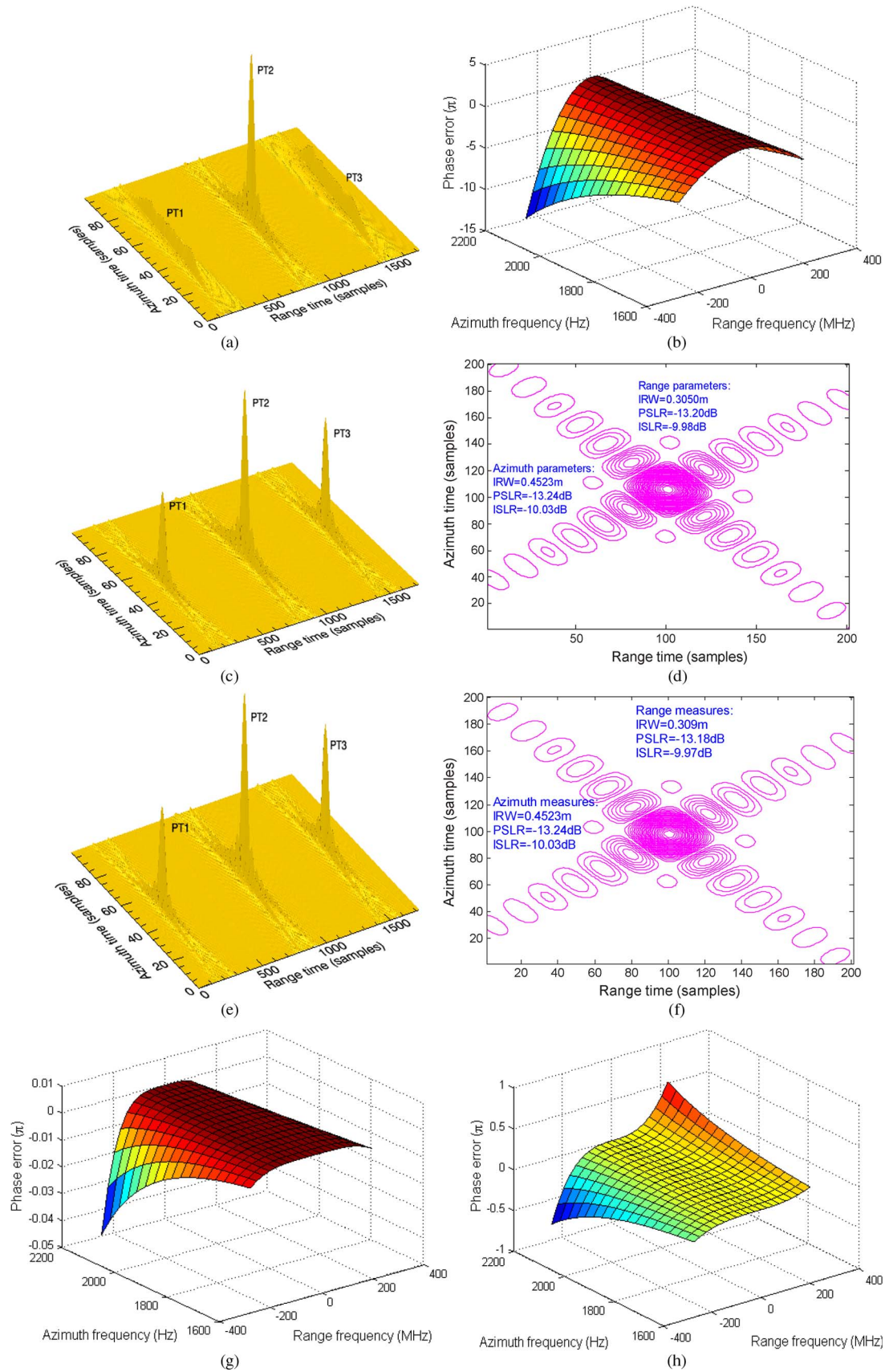


Fig. 5. (a) Focused scene by using the first-order polynomial interpolation transformation. (b) Approximation phase error of the first-order polynomial interpolation transformation in the squint configuration. (c) Focused scene processed using the interpolation transformation of (13) in the squint configuration. (d) Impulse responses of target PT3. (e) Focused scene processed using the interpolation transformation of (20) in the squint configuration. (f) Impulse responses of target PT3. (g) Approximation phase error $\Phi_{E3}(f_a, f)$ of PT3 in the squint configuration. (h) Approximation phase error $\Phi_{E2}(f_a, f)$ of PT3 in the squint configuration.

they are not suitable to process FMCW SAR data in the high-squint case.

2) *Case 2*: The focused result by using (22) is shown in Fig. 5(c). For clarity, PT3 is zoomed and shown in Fig. 5(d).

From the measured parameters shown in Fig. 5(d), IRW broadening is 1.67% in range and 0.84% in azimuth; the degradation in the ISLR is less than 0.3 dB in both directions; and the PSLR agrees well with the theoretical value, which means that the WDA works well in the squint configuration.

3) *Case 3*: This case is to further validate the role of the higher-order phase terms. The phase error introduced by (33) is defined as

$$\begin{aligned} \bar{\Phi}_{E3}(f_\tau, f, r_0) \approx & \frac{4\pi\alpha(r_0 - r_{\text{ref}})}{c} \\ & \times \left[\sqrt{(f_0 + f)^2 - \left[\frac{v}{c}(f_0 + f) + \frac{cf_\tau}{2\alpha v} \right]^2} \right. \\ & - Df_0 - \frac{(1 - \mu_1\mu_2)}{D}f + \frac{(\mu_1 - \mu_2)^2}{2f_0D^3}f^2 \\ & \left. - \frac{(\mu_1 - \mu_2)^2(1 - \mu_1\mu_2)}{2f_0^2D^5}f^3 \right]. \quad (34) \end{aligned}$$

The focused scene is shown in Fig. 5(e). In addition, the zoomed impulse response of PT3 is given in Fig. 5(f).

Comparing this with the results shown in Fig. 5(d), only the range impulse response has little degradation. The range IRW deteriorates with a broadening of 3%, and the range PSLR has a deviation of less than 0.1 dB compared with the theoretical values. Therefore, we conclude that the result with the transformation (33) approximately agrees with the ideal one, which implies that the second- and third-order components play a significant role in the high-squint configuration. For further clarity, we show the approximation phase error $\bar{\Phi}_{E3}(f_\tau, f)$ of PT3 in Fig. 5(g).

From Fig. 5(g), it can be seen that the approximation error $\bar{\Phi}_{E3}(f_\tau, f)$ is negligible. Comparing Fig. 5(b) and (g), it can be seen that the second- and third-order range-azimuth coupling components play a key role in the high-squint configuration. Neglecting them might result in considerable focusing degradation in both directions.

To further highlight the role of the third-order term, the phase error of the second-order polynomial interpolation transformation is shown in Fig. 5(h). The phase error function for the second-order polynomial is formulated as

$$\begin{aligned} \bar{\Phi}_{E2}(f_\tau, f, r_0) \approx & \frac{4\pi\alpha(r_0 - r_{\text{ref}})}{c} \\ & \times \left[\sqrt{(f_0 + f)^2 - \left[\frac{v}{c}(f_0 + f) + \frac{cf_\tau}{2\alpha v} \right]^2} \right. \\ & \left. - Df_0 - \frac{(1 - \mu_1\mu_2)}{D}f + \frac{(\mu_1 - \mu_2)^2}{2f_0D^3}f^2 \right]. \quad (35) \end{aligned}$$

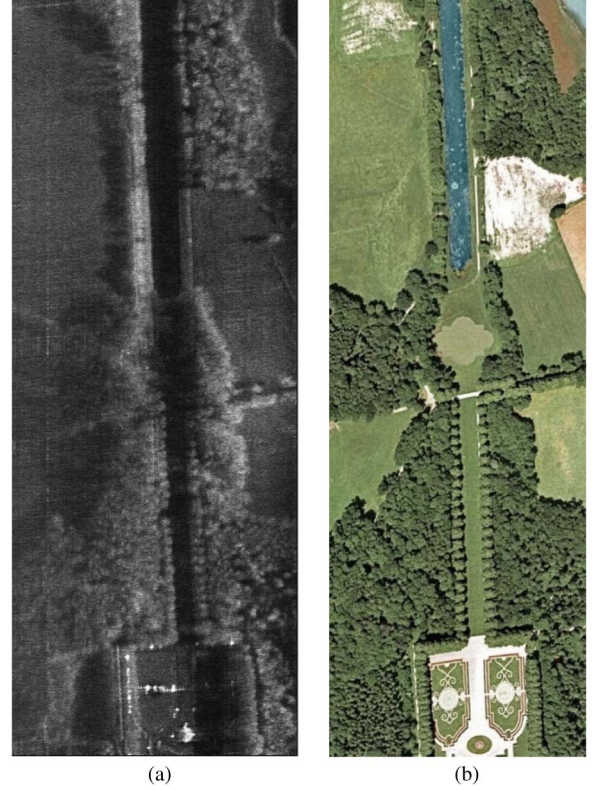


Fig. 6. (a) SAR image processed by the presented algorithm. (b) Optical image from Google Earth. The processed image has a size of 331 m (slant range) \times 897 m (azimuth) at Herrenchiessee, Germany. The horizontal and vertical directions denote the range and the azimuth, respectively.

From Fig. 5(h), it can be seen that the phase error in the second-order model is greater than the acceptable level of $\pi/4$. Therefore, the third-order term in (33) is necessary for this 40° squint case.

V. PROCESSING RESULT OF REAL FMCW SAR DATA

In this section, the signal model and the processing method are validated by real Ka-band FMCW SAR data, which are acquired by using FHR's airborne millimeter-wave SAR system (i.e., MEMPHIS) [13], [14], in April 2008. MEMPHIS is a unique experimental millimeter-wave SAR system that contains two front ends: one operates at 35 GHz (Ka-band) and another at 94 GHz (W-band). The radar system is mounted on a Transall C-160 aircraft with a flight altitude of 320 m, a velocity of 75 m/s, and a looking angle of 70°. For this flight campaign, the minimum slant range is 600 m, and the maximum range is 1000 m. The system has a range bandwidth of 2 GHz and an azimuth Doppler bandwidth of 295 Hz. The corresponding range resolution is 0.075 m, and the azimuth resolution is 0.25 m. It needs to emphasize that a sampling frequency of 25 MHz is applied in the range since the dechirp-on-receive technology is used.

To obtain accurate focusing, the onboard Inertial Navigation System and Global Positioning System are used to collect the information of the position and attitude of the antenna phase center. For this processing, we only implement the range-invariant correction, i.e., the correction for the reference slant

range [11], [15]–[17]. In this paper, we choose the slant range at the middle swath as the reference slant range. Since our real data have a short swath of 400 m, and thus the range-invariant component (i.e., at the reference slant range) is dominant, we neglect the range-variant component for our processing.

By using the proposed signal model and imaging algorithm, the focused SAR image is shown in Fig. 6(a). For comparison, the optical image of the processed scene is shown in Fig. 6(b).

The real Ka-band data are acquired in approximately the broadside case (yaw angle: 2.44°). Therefore, for these real data, the suggested WDA processing does not demonstrate the improved performance since the previous algorithms (i.e., [4], [5], and [7]) can also work well in the broadside case [see Fig. 4(c)].

VI. CONCLUSION

In this paper, we have developed a signal model for the FMCW SAR to address the range variation during the long pulse duration, which is different from the pulsed SAR. Based on the signal model, an analytical PTRS has been developed. Compared with the PTRS of the pulsed SAR, an additional range walk term and a range–azimuth coupling term are found. The range–azimuth coupling term has been disregarded so far in the FMCW SAR community. After RFM to remove the range walk, we use the WDA to focus FMCW SAR data. Simulation experiments show that the WDA can focus FMCW SAR data well in the broadside and high-squint cases. In the high-squint case, it does not require additional computational burden compared with the broadside case. It needs to emphasize that the previous algorithms in [4], [5], and [7] perform well in the broadside case but fail in high-squint cases.

In addition, three interpolation mapping transformations are used to emphasize the role of the range-dependent second- and higher-order range–azimuth coupling components in the high-squint case. Simulations also show that neglecting the higher-order phase terms will result in a significant degradation in both directions. The processing result of the real data shows that the proposed signal model and the processing method can work well in the case of the millimeter-wave FMCW SAR.

ACKNOWLEDGMENT

The authors would like to point out the excellent and very effective cooperation between ZESS and Fraunhofer/FHR, which is seen as a key item of this paper. Finally, the authors would like to thank the anonymous reviewers for their competent and helpful suggestions to improve this paper.

REFERENCES

- [1] J. C. Curlander and R. N. McDonough, *Synthetic Aperture Radar Systems and Signal Processing*. New York: Wiley, 1991.
- [2] G. L. Charvat and L. C. Kempel, "Synthetic aperture radar imaging using a unique approach to frequency-modulated continuous-wave radar design," *IEEE Antennas Propag. Mag.*, vol. 48, no. 1, pp. 171–177, Feb. 2006.
- [3] A. Meta, P. Hoogeboom, and L. P. Ligthart, "Signal processing for FMCW SAR," *IEEE Trans. Geosci. Remote Sens.*, vol. 45, no. 11, pp. 3519–3532, Nov. 2007.

- [4] J. J. M. De Wit, A. Meta, and P. Hoogeboom, "Modified range-Doppler processing for FM-CW synthetic aperture radar," *IEEE Geosci. Remote Sens. Lett.*, vol. 3, no. 1, pp. 83–87, Jan. 2006.
- [5] A. Meta, P. Hoogeboom, and L. P. Ligthart, "Non-linear frequency scaling algorithm for FMCW SAR data," in *Proc. EuRAD*, Manchester, U.K., Sep. 2006, pp. 9–12.
- [6] J. Mittermayer, A. Moreira, and O. Loffeld, "Spotlight SAR data processing using the frequency scaling algorithm," *IEEE Trans. Geosci. Remote Sens.*, vol. 37, no. 9, pp. 2198–2214, Sep. 1999.
- [7] Z. H. Jiang, H. F. Kan, and J. W. Wan, "A chirp transform algorithm for processing squint mode FMCW SAR data," *IEEE Geosci. Remote Sens. Lett.*, vol. 4, no. 3, pp. 377–381, Jul. 2006.
- [8] R. H. Stolt, "Migration by transform," *Geophysics*, vol. 43, no. 1, pp. 23–48, Feb. 1978.
- [9] I. G. Cumming and F. H. Wong, *Digital Processing of Synthetic Aperture Radar Data Algorithms and Implementation*. Norwood, MA: Artech House, 2005.
- [10] W. G. Carrara, R. S. Goodman, and R. M. Majewski, *Spotlight Synthetic Aperture Radar Signal Processing Algorithms*. Boston, MA: Artech House, 1995.
- [11] G. Franceschetti and R. Lanari, *Synthetic Aperture Radar Processing*. Boca Raton, FL: CRC Press, 1999.
- [12] M. Soumekh, "Airborne synthetic aperture acoustic imaging," *IEEE Trans. Image Process.*, vol. 6, no. 11, pp. 1545–1554, Nov. 1997.
- [13] H. Essen, H. Fuchs, and A. Pagels, "High resolution millimeterwave SAR for the remote sensing of wave patterns," in *Proc. IGARSS*, Barcelona, Spain, Jul. 2007, pp. 963–966.
- [14] H. Essen, T. Brehm, M. Hagelen, and H. Schimpf, "Remote sensing at millimetre waves with the MEMPHIS synthetic aperture radar," in *Proc. EUSAR*, Friedrichshafen, Germany, Jun. 2008.
- [15] A. Moreira and Y. H. Huang, "Airborne SAR processing of highly squinted data using a chirp scaling approach with integrated motion compensation," *IEEE Trans. Geosci. Remote Sens.*, vol. 32, no. 5, pp. 1029–1040, Sep. 1994.
- [16] E. C. Zaugg and D. G. Long, "Theory and application of motion compensation for LMC-CW SAR," *IEEE Trans. Geosci. Remote Sens.*, vol. 46, no. 10, pp. 2990–2998, Oct. 2008.
- [17] A. Reigber, E. Alivizatos, A. Potsis, and A. Moreira, "Extended wavenumber-domain synthetic aperture radar focusing with integrated motion compensation," *Proc. Inst. Elect. Eng.—Radar Sonar Navig.*, vol. 153, no. 3, pp. 301–310, Jun. 2006.



Robert Wang (M'07) received the B.S. degree in control engineering from the University of Henan, Kaifeng, China, in 2002 and the Dr. Eng. degree from the Graduate University of the Chinese Academy of Sciences, Beijing, China, in 2007.

In 2007, he joined the Center for Sensorsystems (ZESS), University of Siegen, Siegen, Germany, where he is currently working on the hybrid bistatic experiment. He was also involved in some SAR projects for the Fraunhofer Institute for High Frequency Physics and Radar Techniques (FHR). He has

contributed to invited sessions on bistatic SAR at the European Conference on Synthetic Aperture Radar (EUSAR) 2008. He is the author of a tutorial entitled "Results and progresses of advanced bistatic SAR experiments" presented at the European Radar Conference 2009 and the coauthor of a tutorial entitled "Progress in bistatic SAR concepts and algorithms" presented at EUSAR 2008. His current research interests include monostatic and bistatic SAR signal processing, bistatic interferometric, airborne SAR motion compensation, FMCW SAR systems, and millimeter-wave SAR systems.



Otmar Loffeld (M'05–SM'06) received the Diploma degree in electrical engineering from the Technical University of Aachen, Aachen, Germany, in 1982 and the Eng. Dr. degree and the “Habilitation” degree in the field of digital signal processing and estimation theory from the University of Siegen, Siegen, Germany, in 1986 and 1989, respectively.

In 1991, he was appointed Professor of digital signal processing and estimation theory with the University of Siegen. Since then, he has been giving lectures on general communication theory, digital signal processing, stochastic models and estimation theory, and synthetic aperture radar. He is the author of two textbooks on estimation theory. In 1995, he became a member of the Center for Sensorsystems (ZESS), which is a central scientific research establishment at the University of Siegen. Since 2005, he has been the Chairman of ZESS. In 1999, he became a Principal Investigator (PI) on baseline estimation for the X-band part of the Shuttle Radar Topography Mission (SRTM), where ZESS contributed to the German Aerospace Center (DLR)'s baseline calibration algorithms. He is a PI for interferometric techniques in the German TerraSAR-X mission, and, together with Prof. Ender from FGAN, he is one of the PIs for a bistatic spaceborne airborne experiment, where TerraSAR-X serves as the bistatic illuminator, whereas the Fraunhofer Institute for High Frequency Physics and Radar Techniques (FHR)'s PAMIR system mounted on a Transall airplane is used as a bistatic receiver. In 2002, he founded the International Postgraduate Programme (IPP) “Multi Sensorics.” In 2008, based on the aforementioned program, he established the “NRW Research School on Multi Modal Sensor Systems for Environmental Exploration and Safety (MOSES)” at the University of Siegen as an upgrade of excellence. He is the Speaker and Coordinator of both doctoral degree programs, which are hosted by ZESS. Furthermore, he is the university's Scientific Coordinator for “Multidimensional and Imaging Systems.” His current research interests comprise multisensor data fusion, Kalman filtering techniques for data fusion, optimal filtering and process identification, SAR processing and simulation, SAR interferometry, phase unwrapping, and baseline estimation. His recent field of interest is bistatic SAR processing.

Dr. Loffeld is a member of the Information Technology Society (ITG) of the German Association for Electrical, Electronic and Information Technologies (VDE) and a Senior Member of the IEEE Geoscience and Remote Sensing Society. He was the recipient of the Scientific Research Award of North Rhine-Westphalia (“Bennigsen-Foerder Preis”) for his works on applying Kalman filters to phase estimation problems such as Doppler centroid estimation in SAR, phase, and frequency demodulation.



Holger Nies received the Diploma degree in electrical engineering and the Dr. Eng. degree from the University of Siegen, Siegen, Germany, in 1999 and 2006, respectively.

Since 1999, he has been a member of the Center for Sensorsystems (ZESS), University of Siegen, and a Lecturer with the Department of Signal Processing and Communication Theory. He worked in the project sector “Optimal Signal Processing, Remote Sensing—SAR” of ZESS in 1999. He was also involved in some project work for Daimler AG, Stuttgart, Germany, in the field of engine modeling and optimization. He is currently working in the area of interferometric techniques in the German TerraSAR-X mission. He is a Principal Investigator on the development of a stationary receiver SAR system for acquiring and processing signals transmitted from the TerraSAR-X satellite. His current research interests include bistatic SAR processing, SAR interferometry, and distributed data fusion.

Dr. Nies was the recipient of the “Best Poster Award” at the European Conference on Synthetic Aperture Radar (EUSAR) 2006, Dresden, Germany.



Stefan Knedlik (M'04) received the Diploma degree in electrical engineering and the Dr. Eng. degree from the University of Siegen, Siegen, Germany, in 1998 and 2003, respectively.

Since 1998, he has been a member of the Center for Sensorsystems (ZESS), University of Siegen, and since 2003, he has also been a Researcher/Assistant Professor (C1) with the Institute of Signal Processing and Communication Theory, Department of Electrical Engineering and Computer Science. He is also an Executive Director of two international postgraduate programs: the International Postgraduate Programme (IPP) Multi Sensorics and the Research School on Multi Modal Sensor Systems for Environmental Exploration and Safety (MOSES). A few years ago, he founded a research group on navigation. His current research interests include GNSS-based navigation, inertial navigation, sensor data fusion, and signal processing in synthetic aperture radar interferometry.



Manfred Hägelen received the Diploma degree in electrical engineering from the Technical University of Brunswick, Brunswick, Germany, in 2003. He is currently working toward the Ph.D. degree with the International Postgraduate Programme Multi Sensorics, Center for Sensor Systems (ZESS), University of Siegen, Siegen, Germany.

Since January 2003, he has been a Research Associate with the Fraunhofer Research Institute for High Frequency Physics and Radar Techniques (FHR), Wachtberg, Germany. In September 2009, he became a Team Leader of Sensor Systems for Security Applications with the Department of Millimeter Wave Radar and High Frequency Sensors. His current research interests include multiple-sensor systems, FMCW SAR signal processing, airborne SAR motion compensation, FMCW SAR systems, and millimeter-wave radar systems.



Helmut Essen received the Diploma degree in physics and the Ph.D. degree from the University of Bonn, Bonn, Germany, in 1973 and 1976, respectively.

He was with the Max-Planck-Institute for radio-astronomy, where he was engaged in the development of millimeter-wave radiometers, until 1977. Since then, he has been with the Fraunhofer Research Institute for High Frequency Physics and Radar Techniques (FHR), Wachtberg, Germany, as a Research Scientist and Group Leader, engaged in the development of millimeter-wave radar in the frequency range of 10–220 GHz. Since 1995, he has been heading the Department of Millimeter Wave Radar and High Frequency Sensors. His work on target background signatures covered experimental investigations and the development of signal processing algorithms using SAR, InSAR, and ISAR. His further fields of research have been propagation of radio waves and terahertz imaging for security applications.

Dr. Essen is a member of the German Physical Society (DPG), the German Terahertz Center, and the IEEE Geoscience and Remote Sensing Society.